Specific Developments on a Finite Element Tool for Thin Crack Modelling in EC Testing

Yahya CHOUA, Laurent SANTANDREA, Yann LE BIHAN and Claude MARCHAND,
LGEP, Gif-sur-Yvette Cedex, France

Abstract. The finite element modelling of thin cracks in ECT using **a**-ψ and **t**-ϕ combined vector-scalar potential formulations is presented with edge and nodal Whitney element discretization. The crack is treated as a non-conductive surface on which appropriate conditions are applied to comply with the right behaviour of the field quantities. The implementation of the two formulations is based on the object-oriented programming. Several problems have been solved to validate the model.

1. Introduction

Eddy current testing (ETC) is widely used for detecting defects in metallic components. Usually the modelling of an ECT configuration cannot be obtained analytically and requires the use of 3-D numerical methods. Among them, the finite element method (FEM) appears to be very powerful because of its large flexibility which allows to take into consideration complex configurations. Nevertheless the FEM modeling of thin insulating cracks in ECT requires a high density mesh which increases the computation time and can lead to highly deformed elements and consequently an ill-conditioned system. This drawback can be avoided by considering a thin insulating crack as a non-conductive surface. In this case, the energy term associated to this crack is neglected and appropriate boundary conditions are applied [1]-[2]. Within the framework of the European project VERDICT, the ECT modeling of thin cracks has been studied using combined potential formulations with the vector and scalar degrees of freedom discretized by edge and nodal Whitney elements, respectively [3].

2. Description of the approaches

2.1 Introduction

A typical ECT problem is shown in Fig. 1. The study domain Ω, includes a conducting domain Ω_c in which exists a thin crack having a surface S_f. The probe is constituted of a coil driven by an excitation current density $\mathbf{j_0}$ and may include a magnetic core. On the boundary, $\partial\Omega = \Gamma_e \cup \Gamma_h$, with $\Gamma_e \cap \Gamma_h = \varnothing$, we have $\mathbf{n} \times \mathbf{e} = \mathbf{0}$ on Γ_e and $\mathbf{n} \times \mathbf{h} = \mathbf{0}$ on Γ_h, respectively, with $\mathbf{n}$ the normal of $\partial\Omega$.

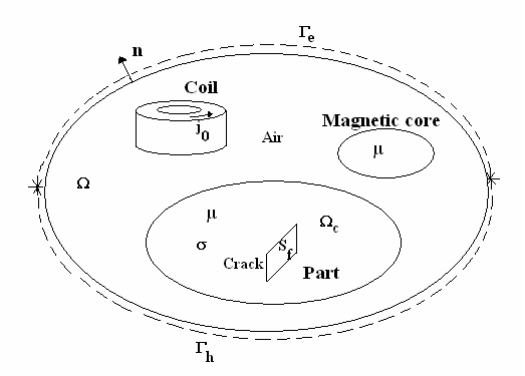

Fig. 1. ECT problem

The crack is treated as a nonconducting surface. As a consequence, the current density has to satisfy on S_f:

$$\mathbf{j}.\mathbf{n_c} = 0 \qquad (1)$$

where $\mathbf{n_c}$ and $\mathbf{j}$ are the normal of the crack surface and the current density, respectively. Moreover through the crack surface the tangential component of the current density $\mathbf{j}$ is usually not continuous (Fig. 2.):

$$[\mathbf{j}] = \mathbf{j}^+ - \mathbf{j}^- \neq \mathbf{0} \qquad (2)$$

where [.] denotes the jump of a quantity i.e., the difference between the values of the quantity on the opposite sides of the crack surface.

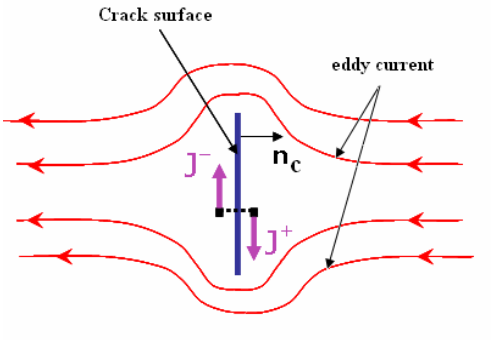

Fig. 2. Effect of the crack on the current density

With the implemented approach, the crack is not meshed by finite elements, but its surface is discretized by the facets of volumic elements of the mesh (so, no element cross the crack). Fig. 3 shows an example of discretization of the surface of a crack by element facets.

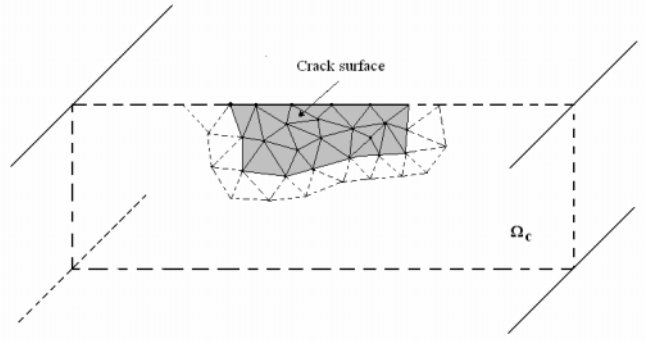

Fig. 3. Crack discretization by finite element facets

The problem can be solved by FEM using either a magnetic formulation in terms of the combined vector-scalar potentials **t**-ϕ where, **t** is the electric vector potential and ϕ is the magnetic scalar potential, or an electric formulation in terms of **a**-ψ where **a** and ψ are the magnetic vector potential and a time primitive of the electric scalar potential, respectively [3]. The mesh is based on first order edge and nodal Whitney tetrahedral elements. Fig.4 shows a Whitney tetrahedral element.

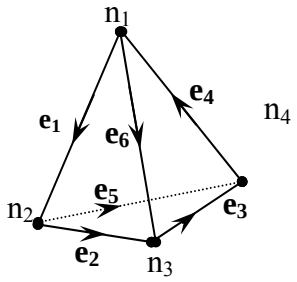

Fig. 4. Tetrahedral Whitney element

The degrees of freedom ϕ and ψ (scalar potentials) are discretized at the nodes (n_i) i =1 to 4 and the circulations of **a**, **t** (vector potentials) are discretized at the edges $\mathbf{e}_i$ i =1 to 6. Thanks to the properties of Whitney elements, the electric formulation approximates strongly the Faraday law whereas the ampere law is weakly approximated. On opposite the Ampere law is strongly approximated by the magnetic formulation whereas the Faraday law is weakly approximated. The duality between the magnetic and the electric formulations can be used for an adaptive mesh refinement for 3D ECT problems using the principle of Ligurian [4]. The implementation of both formulations is presented in what follows.

*2.2 Electric formulation **a**-ψ*

The electric field **e** is expressed by:

$$\mathbf{e} = -\partial_t(\mathbf{a} + \text{grad}\ \psi) \qquad (3)$$

where ∂_t denotes the derivation in time.
From (2), it results that the tangential component $\mathbf{e}_t$ of the electric field is not continuous through the crack surafce.

$$[\mathbf{e}_t] = -\partial_t([\mathbf{a}_t] + \text{grad}_t\,[\psi]) \neq \mathbf{0} \qquad (4)$$

where $\mathbf{a}_t$ is the tangential component of the magnetic vector potential and grad_t denotes the tangential component to the crack surface of the gradient. However, the continuity of the normal component of the magnetic induction through the crack implies that: $\mathbf{n_c}.\text{curl}[\mathbf{a}] = 0$. It follows that a possible discontinuity of the tangential component $\mathbf{a}_t$ of **a** is only due to a surface gradient of a scalar field α:

$$[\mathbf{a}_t] = \text{grad}_t\ \alpha \qquad (5)$$

This discontinuity can be transfered in a jump of ψ. Consequently, the jump of the tangential component of the electric field is treated by setting $\mathbf{a}_t$ continuous (no special treatment on the element edges) and allowing a jump of ψ:

$$[\mathbf{e}_t] = -\partial_t(\text{grad}_t\,[\psi]) \neq \mathbf{0} \qquad (6)$$

Therefore, the nodal degrees of freedom ψ attached to the crack surface are duplicated on the left and right sides of S_f.

*2.3 Magnetic formulation **t**-ϕ*

With the **t**-ϕ magnetic formulation, the magnetic field **h** is given by:

$$\mathbf{h} = \mathbf{t} + \text{grad}\,\phi \qquad (7)$$

in the conducting domain Ω_c.
In the nonconducting domain $\Omega\backslash\Omega_c$ the magnetic field is expressed by: $\mathbf{h} = \text{grad}\,\phi$. The current density, $\mathbf{j} = \text{curl}\,\mathbf{t}$, satisfies on the crack surface to:

$$\mathbf{n_c}.\text{curl}\,\mathbf{t} = 0 \qquad (8)$$

It follows that the tangential component to the crack surface $\mathbf{t}_t$ of the electric vector potential is a surface gradient of a scalar field ξ:

$$\mathbf{t}_t = \text{grad}_t\,\xi \qquad (9)$$

This gradient term can be transfered in gradient term of ϕ i.e the electric vector is normal to crack surface. So, (8) can be verified by setting to zero the circulation of the electric vector potential along the edges belonging to the crack surface.

2.4 Probe signal calculation

Considering a sinusoidal excitation, the variation of the impedance ΔZ of the probe due to the crack is calculated from the Joule-losses and the stored magnetic energy. The real part of the impedance change is obtained as:

$$I^2\,\text{Re}(\Delta Z) = \int_{\Omega_c} \frac{1}{\sigma}\left(|\mathbf{j_f}|^2 - |\mathbf{j}|^2\right) d\Omega \qquad (10)$$

and the imaginary part is given by :

$$I^2\,\text{Im}(\Delta Z) = \omega \int_{\Omega} \frac{1}{\mu}\left(|\mathbf{b_f}|^2 - |\mathbf{b}|^2\right) d\Omega \qquad (11)$$

where **j** and **b** denote the current density and the magnetic induction without flaw, respectively. $\mathbf{j_f}$ and $\mathbf{b_f}$ are the current density and the magnetic induction with flaw, respectively. I is the excitation current in the coil. μ and σ are the permeability and the conductivity of the part, respectively. ω denotes the pulsation.

3. Software consideration

The mathematical approach is integrated in our laboratory research code. This 3D finite elements code is based on the object-oriented programming (OOP) paradigm. It is implemented in C++ language which exhibits its advantages such as standardization, speed and flexibility (using of templates).
One important feature is the capability of dealing with matrix object. This matrix object is based on an abstract class which uses mathematical structures of linear algebra. In particular, this object-oriented structure allows an easy management of the degrees of freedom which simplifies the implementation of the FEM formulations. The computational time of FEM resolution can be important. It is obvious that computational effort becomes prohibitive if we want to optimise the probe or to reconstruct the flaw (inverse problem). To overcome this difficulty parallel computing can be used [5]. Dual-processors with hyper-threading technology is became a current architecture, and can be obtained with a very reasonable cost. A simple technique based on OpenMP (Open Multi Processing) has been carried out to obtain a significant speed-up of the numerical simulation code and to exploit this machine architecture.

4. Results

4.1 ECT configuration

Several benchmark problems have been considered in order to validate the **a**-ψ and **t**-ϕ formulations. A circular cored coil is displaced parallel to the y-axis (see Fig. 5), along the length of a rectangular slot in a plate. Both frequency and coil lift-off are fixed and the impedance variation is measured as a function of the position of the coil-center.

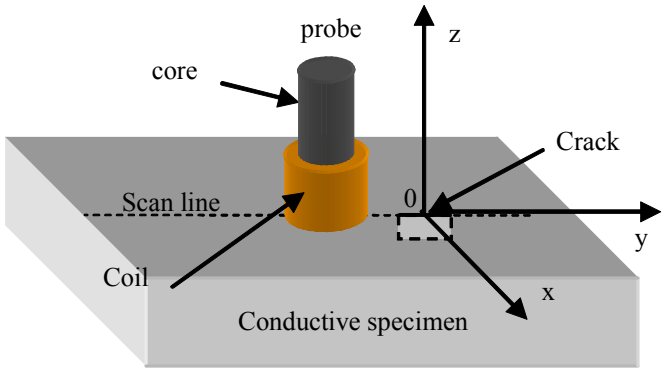

Fig. 5. ECT configuration

The objective is to compute the change of the impedance of the coil (compared to its value over an unflawed portion of the plate) as a function of coil position, and to compare the computed results to the experimental ones.

4.2 JSAEM benchmark problem

The different parameters of JSAEM n° 2-5 problem are listed in table 1.

Table 1
Parameters of the JSAEM problem

Probe	
Inner radius (mm)	0.6
Outer radius (mm)	1.6
Length (mm)	0.8
Relative permeability	1
Number of turns	140
Lift-off (mm)	0.5
Frequency (Hz)	150×10^3
Plate	
Conductivity (S/m)	1.0×10^6
Thickness (mm)	1.25
Crack	
Length (mm)	10.0
Depth (mm)	0.75
Width (mm)	0.21

Fig. 6 shows the variation of the reactance and of the resistance of the probe versus the probe position along the crack length. The crack is centred at y = 0.

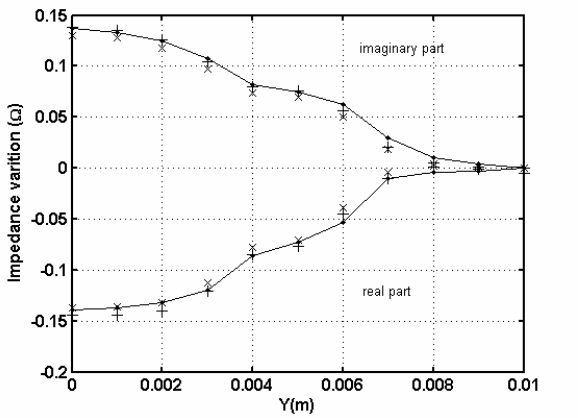

Fig. 6. Variation of the probe impedance **a**-ψ (+), **t**-ϕ (x) and experimentation (—).

4.3 TEAM benchmark problem

The different parameters of TEAM workshop n° 15-1 problem [6] are listed in table 2.

Table 2
Parameters of the TEAM problem

Probe	
Inner radius (mm)	6.15
Outer radius (mm)	12.4
Length (mm)	6.15
Relative permeability	1
Number of turns	3790
Lift-off (mm)	0.88
Frequency (Hz)	900
Plate	
Conductivity (S/m)	30.6×10^6
Thickness (mm)	12.22
Crack	
Length (mm)	12.6
Depth (mm)	0. 5
Width (mm)	0.28

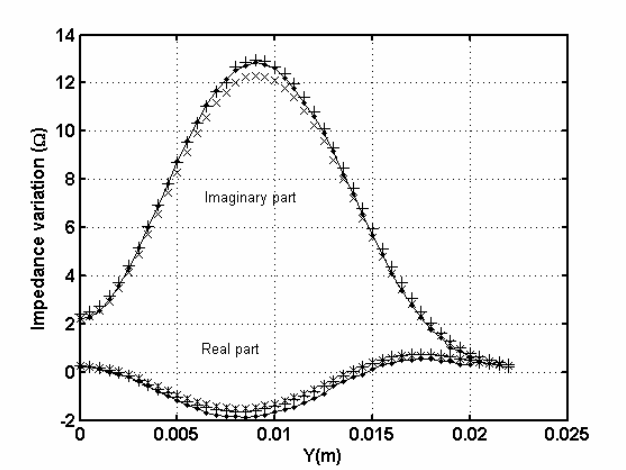

Fig. 7. Variation of the probe impedance: **a**-ψ (+), **t**-ϕ (x) and experimentation (—).

Fig. 7 shows the comparison between calculated and experimental signals.

4.4 Small Flaw Problem

The considered problem is a rectangular flawed part scanned by a probe constituted of a circular coil wound around a ferrite stick. The different parameters of the problem are listed in table 3.

Table 3
Parameters of the small flaw problem

Probe		
Coil inner radius (mm)	0.4	
Coil outer radius (mm)	0.6	
Coil length (mm)	1.4	
Coil number of turns	110	
Core length (mm)	1.4	
Core relative permeability	1100	
Lift-off (μm)	20	
Frequency (Hz)	2×10^6	
Plate		
Conductivity (S/m)	0.76×10^6	
Thickness (mm)	3	
Cracks		
Length (mm)	0.4	0.8
Depth (mm)	0.2	0.1
Width (mm)	0.1	0.1

Fig. 6 and Fig. 7 show the comparison between calculated and measured signals along the y-axis (x=0) for two different cracks.

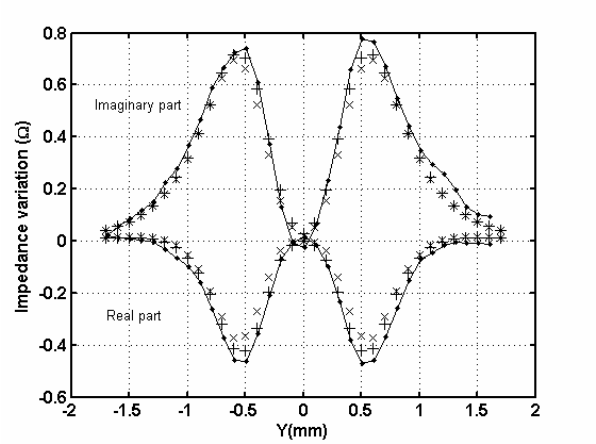

Fig. 7. Variation of the probe impedance (crack: 0.4 mm x 0.2 mm)): **a**-ψ (+), **t**-ϕ (x) and experimentation (—).

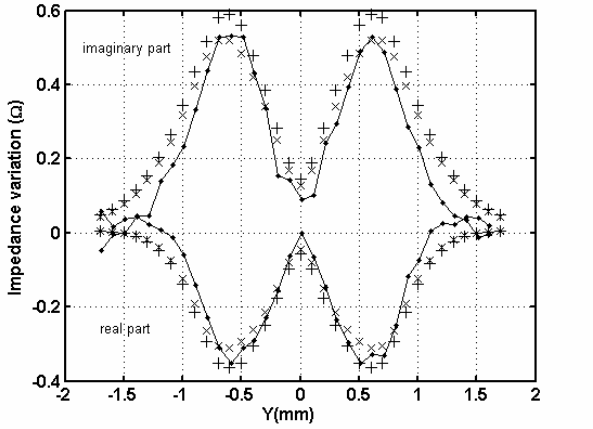

Fig. 8. Variation of the probe impedance (crack: 0.8 mm x 0.1 mm)): **a**-ψ (+), **t**-ϕ (x) and experimentation (—).

5. Conclusion

This paper presents specific developments on a finite element tool for solving ECT problems in presence of crack using a combined potential formulation with edge and nodal Whitney elements. For the different problems treated a good agreement is obtained between the numerical results and the experimental ones. The two proposed approaches allow an efficient and accurate calculation of the signal induced by the interaction of ECT probes and cracks with a reduced and less crucial mesh comparatively to an usual volumic meshing of the crack. The accuracy of the model has been highlighted by comparing calculation and experimentation for different crack sizes. The method has been implemented on rectangular crack problems in order to validate the approach but it can be applied to more complex probe, part and crack configuration (e.g.: non planar crack).

6. Acknowledgements

This work was supported by the European Community within the framework of the project VERDICT (contract n^{o} G4RD-CT-2002-00860).

7. References

[1] A. Bossavit “Small parameter problems in eddy-current theory: a review, and a case-study on how to avoid meshing small air-gaps”, IEEE Trans. Mag. Vol. 32, No. 3, 1996, pp.729-732

[2] P. Dular and C. Geuzaine "Modeling of thin insulating layers with dual 3-D magnetodynamic formulations" IEEE Trans. Mag., vol 39, No.53, 2003, pp.1139-1142.

[3] Z. Ren and A. Razek. “Computation of 3-D Electromagnetic Field Using Differential Forms Based Elements and Dual Formulations”, International Journal of Numerical Modelling , vol.9, 1996, pp. 81-98

[4] C. Li, Z. Ren and A. Razek “An approach to adaptive mesh refinement for three-dimensional eddy-current computations”, IEEE Tran. Mag. Vol. 30, No. 1, 1994, pp 113-117

[5] L. Santandrea, G. Savel, Y. Le Bihan and A. Razek “Parallel computing for eddy current testing simulation” CEM 2006 Aachen.

[6] S. K. Burke, “A benchmark problem for computation of ΔZ in eddy-current nondestructive evaluation (NDE)” J. Nondestructive Evaluation, Vol. 7, Nos. 1/2, 1988, pp 35-41